ADVANCED FUNCTIONAL MATERIALS
www.afm-journal.de

Multi-Photon 3D Laser Micro-Printed Plastic Scintillators for Applications in Low-Energy Particle Physics

Jannis Weinacker, Sebastian Kalt, Anton Huber, Nathanael Gutknecht, Jonathan Ludwig Günter Schneider, Niclas Maximilian Bojanowski, Tom Geigle, Markus Steidl, and Martin Wegener**

Plastic scintillators are inexpensive to manufacture and therefore a popular alternative to inorganic crystalline scintillators. For many applications, their advantages outweigh their lower light yield. Additionally, it is easier to structure plastic scintillators with well-developed processing techniques which is of growing relevance in modern applications. One technique to structure plastic material is 3D printing, with noteworthy recent advances in one-photon-based approaches. However, some applications require high spatial resolution and optically smooth surfaces, which can be achieved by multi-photon 3D laser micro-printing. One application example is the improvement of sensitivity of the Karlsruhe Tritium Neutrino (KATRIN) experiment. This improvement can be realized by printing a 3D scintillator structure as an active transverse energy filter directly onto the detector. Herein, the first two-photon printable plastic scintillator providing a printing resolution in the micrometer regime is presented. Using the benefits of two-photon grayscale lithography, optical-grade surfaces are achieved. The light output is estimated to be 930 photons MeV^{-1}. A prototype structure printed directly on a single-photon avalanche diode array is demonstrated.

1. Introduction

Since the late 1970s, plastic scintillators have been widely used in particle physics[1] and are still a state-of-the-art technology used, for example, as calorimeters in collider experiments[2–5] as well as in the field of neutrino physics,[6–8] or medical applications.[9–12] A growing number of detector systems require a direct connection between the scintillator and the photodetector[13,14] as well as precise control over the shape of the scintillator itself.[15,16] Both requirements can be fulfilled by 3D printing of a plastic scintillator onto the detector.[17–19] However, state-of-the-art one-photon-based 3D printing approaches, with a linear relation between dose and intensity, for scintillators suffer from insufficient spatial resolution for applications relying on scintillating microstructures.[20]

In contrast to linear one-photon 3D printing, the nonlinear multi-photon laser micro-printing approach provides a significantly higher resolution and full 3D printing capability.[21] Additionally, techniques such as two-photon grayscale lithography (2GL)[22] enable the fabrication of microstructures with optical-surface quality,[23,24] which can be crucial for light-emitting structures such as scintillators. In particular, total internal reflection to waveguide the generated light critically depends on high-quality surfaces. Lastly, by means of 3D laser micro-printing, one can print directly onto many different surfaces, allowing, e.g., to directly print the scintillator onto (photo)diodes[25] or fiber tips.[26–29]

In this work, we present the first plastic scintillator that can be 3D printed using two-photon absorption. In particular, we demonstrate the 2GL-printing capabilities of naphthyl- and bisphenol-based resins, which are inspired by one-photon printing,[18] with structures showing micrometer-sized features. The printed scintillator's efficiency is measured using a scanning electron microscope (SEM) including a luminescence detector by comparing it with a commercially available plastic scintillator. Additionally, we present a potential detector system acting as an active-transverse-energy filter (aTEF)[20] applicable in large particle physics experiments such as the Karlsruhe Tritium Neutrino (KATRIN) experiment. We demonstrate the printability of such

J. Weinacker, S. Kalt, J. L. G. Schneider, N. M. Bojanowski, M. Wegener
Institute of Applied Physics (APH)
Karlsruhe Institute of Technology (KIT)
Wolfgang-Gaede-Str. 1, 76131 Karlsruhe, Germany
E-mail: jannis.weinacker@kit.edu; martin.wegener@kit.edu

J. Weinacker, S. Kalt, J. L. G. Schneider, N. M. Bojanowski, M. Wegener
3DMM2O-Cluster of Excellence
Karlsruhe Institute of Technology (KIT) and Heidelberg University
76128 Karlsruhe, Germany

A. Huber, M. Steidl
Institute for Astroparticle Physics (IAP)
Karlsruhe Institute of Technology (KIT)
Hermann-von-Helmholtz-Platz 1, 76344 Eggenstein-Leopoldshafen, Germany

N. Gutknecht, T. Geigle
Institute of Experimental Particle Physics (ETP)
Karlsruhe Institute of Technology (KIT)
Wolfgang-Gaede-Str. 1, 76131 Karlsruhe, Germany

The ORCID identification number(s) for the author(s) of this article can be found under https://doi.org/10.1002/adfm.202413215

DOI: 10.1002/adfm.202413215

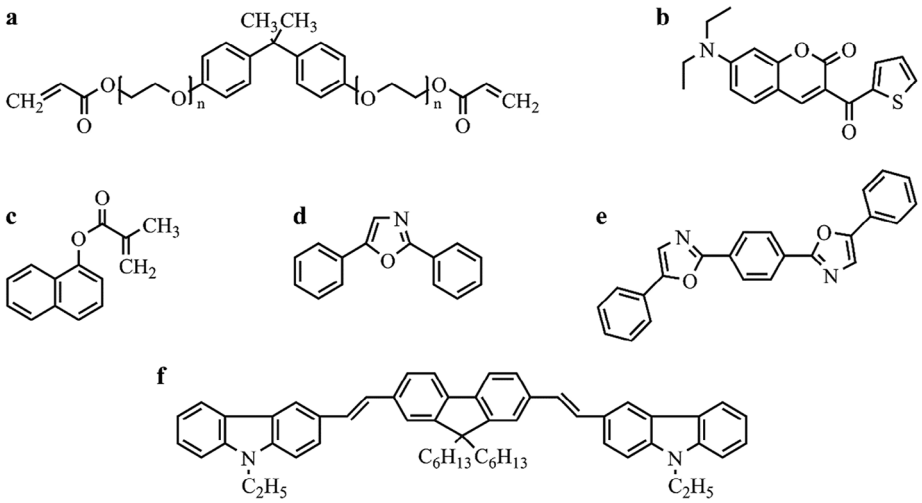

Figure 1. Chemical structural formulas of the components of the scintillator resin. The molecules are Bisphenol A ethoxylate diacrylate (a), DETC or 7-diethylamino-3-thenoylcoumari (b), 1-Naphthyl methacrylate (c), PPO or 2,5-Diphenyloxazole (d), POPOP or 1,4-bis(5-phenyloxazol-2-yl) benzene (not used in the recipe) (e), and ADS086BE or 1,4-Bis(9-ethyl-3-carbazo-vinylene)-9,9-dihexyl-fluorene (f).

a scintillator detector in an aTEF geometry directly on a single-photon avalanche diode array (SPAD-array). By reading out the corresponding SPADs,[30] this composition could act then as a complete functional detector system.

2. Fabrication Methods

In the following, we present the complete fabrication routine for our 3D-printed scintillator. We start by describing the composition of the resin and the mixing procedure and continue with the 3D printing device as well as the settings for the printing process.

2.1. Resin Composition

In general, a plastic scintillator consists of a polymer matrix, a scintillating material, and wavelength shifters. While the matrix guarantees structural stability, the scintillating material emits the light induced by the energy deposit of an incoming particle. For this process, aromatic systems are particularly interesting due to the large number of delocalized electrons. To suppress reabsorption by the scintillating molecules, the wavelength shifter absorbs the generated photons and reemits them at a larger wavelength through a fluorescence process. This wavelength-shifted light can then be transmitted through the scintillator material without being reabsorbed again. Commercially available resists for two-photon absorption (2PA) or 2GL are mainly based on (meth)acrylates due to their efficient polymerization rate.[31,32] A challenge we faced is the low solubility with an increased size of the aromatic core, while any remaining solid or crystal in the liquid acrylates induces scattering and micro explosions due to the high 2PA of aromatic units.

As polymer matrices, we tested the commercially available two-photon photoresin IP-S NPI (NPI for "no photoinitiator") from Nanoscribe and the monomer Bisphenol A ethoxylate diacrylate (see chemical structure in **Figure** 1a) with a molar mass of 468 g mol^{-1}. We later found that the scintillation efficiency of the polymer consisting of the latter monomer is significantly higher. The choice of the monomer is consistent with the idea that aromatic systems in the matrix also increase the scintillation efficiency.[19] As a photoinitiator, we use DETC[33–35] (7-diethylamino-3-thenoylcoumari, Figure 1b) with a concentration of 0.34 w.%. To increase the scintillation efficiency, we add 1-Naphthyl methacrylate (Figure 1c) as a second monomer as suggested in the literature[18] with 20 w.%. This concentration results from a trade-off. A higher concentration of this component leads to difficulties during the printing process, an insufficient degree of polymerization, and therefore also insufficient mechanical stability of the final structures (mechanical properties are shown in the Section S2, Supporting Information). Lower concentrations, however, reduce the scintillation efficiency. A comparison of the overall performance of three different concentrations of 1-Naphthyl methacrylate is shown in Figure S4 (Supporting Information). The last components are the wavelength shifters. Here, PPO (2,5-Diphenyloxazole, see structure in Figure 1d) is used to shift the light emitted by the scintillation process from the UV to the blue spectral region. To shift the wavelength even further closer to the green spectral region, a second wavelength shifter is required. A common choice in this context is POPOP (1,4-bis(5-phenyloxazol-2-yl) benzene, see chemical structure in Figure 1e). This compound, however, is highly insoluble in many organic monomers and does not show a better performance than ADS086BE (1,4-Bis(9-ethyl-3-carbazo-vinylene)−9,9-dihexyl-fluorene, see chemical structure in Figure 1f). For this reason, we chose ADS086BE to perform the second wavelength shift.

2.1.1. Photoresin Mixing Procedure

The optimized resin is composed of 1-Naphthyl methacrylate and the two wavelength shifters. PPO (1.5 w.%) and ADS086BE (0.08 w.%) were dissolved in the melted 1-Naphthyl methacrylate

(20 w.%) at 60 °C under constant stirring of 1 h. Next, the photoinitiator (0.34 w.%) and the Bisphenol A ethoxylate diacrylate were added, such that all components add up to 100 w.%. Last, the resin was again heated and stirred at 60 °C until the photoinitiator dissolved. Finally, the resin was filtered using a 200 nm filter.

2.2. 3D Printing Process

The scintillator is printed using a Nanoscribe QuantumX exploiting the benefits of 2GL. This printer is equipped with a femtosecond-pulsed laser with a repetition rate of 80 MHz and a pulse duration below 150 fs at a center wavelength of 780 nm. While in the past this printing technology delivered optical grade surface qualities only for 2.5D micro-optical components,[22] in the recent past an update was launched that transfers this ability to truly 3D structures. Thus, it is now possible to print fully 3D objects including overhanging features with smooth surface qualities. This advance is highly beneficial for 3D-printed scintillators as the light will interact with the surface in a controllable way.

For the printing process a 25×/NA = 0.8 objective lens was used as the print head in dip-in mode as intended in the "medium-feature set". On the machine, the nanoSQX version 4.0.11 was installed and the job files were generated with NanoPrintX (version 4.0.2) for 3D structures without stitching or GrayScribeX (version 4.0.1) for 2.5D structures including stitching. While the scan speed was chosen to be at the maximum of 25 $cm^{-1}s^{-1}$, hatching, and slicing were set to smaller values of 500 nm slicing and 100 nm hatching to get good resolution despite a very pronounced proximity effect. Given these three values, the laser power was optimized to 38 mW to achieve sufficient polymerization while avoiding micro-explosions in the resin.

Next, we determined the 2GL parameters. Therefore, the number of layers was chosen to be 5 which is a common value recommended by Nanoscribe.[36] This is equivalent to a multilayer attenuation of 0.8 in GrayScribeX. A sweep for the parameters "minimum power" (from 0 to 12 mW in steps of 1 mW) and "power exponent" (from 1.0 to 2.0 in steps of 0.1) was performed by printing small lenses with a radius of 130 µm, a height of 60 µm, and a curvature of 0.01 $µm^{-1}$. As suggested in the Nanoguide[36] from Nanoscribe for the determination of 2GL parameters for custom resins, the analysis of the printed lenses was performed using a spinning-disk confocal-optical microscope (MarSurf CM explorer S/W, Mahr GmbH). Promising results were found for a minimum power of 8 mW and a power exponent of 1.5. Here, the maximum height value was 23.3 nm, after applying a bandpass filter from 2.5 to 8 µm to the measured topography profile. This value can be interpreted as a roughness value. Lastly, the "mesh z offset" was determined and good results were found for 1.9 µm.

After exposure, the structure is developed first in a bath of propylene glycol methyl ether acetate (PGMEA) for 20 min. Next, we rinsed the sample with isopropanol followed by another bath in fresh isopropanol for another 5 min. Finally, the sample is rinsed a second time with isopropanol and blown dry with pressured nitrogen gas.

3. Characterization of the Scintillation Efficiency

Typically, 3D-printed scintillators are tested using a photomultiplier tube and an electron source to generate a signal.[17–19] However, for our small scintillator samples this approach is not suitable since the covered area of the photomultiplier tube is too small. Therefore, the scintillator would be hit only by a small number of particles resulting in a too small number of detectable events. To circumvent this issue, we use a scanning electron microscope (Zeiss Supra 55VP) to hit the sample with electrons of known energy. A photomultiplier (VPSE detector) in the chamber collects the emitted light and gives information about the scintillation capabilities.

3.1. Qualitative Demonstration of the Scintillation in Comparison with IP-S

First, we would like to demonstrate the scintillator's capabilities in comparison with the commercial photoresist IP-S from Nanoscribe. Therefore, we printed a chessboard where all black fields and figures were printed with IP-S, whereas the white fields and figures were printed with our scintillator resin. For IP-S, we used the standard parameters suggested by Nanoscribe (slicing 1 µm, hatching 200 nm, scan speed 25 $cm^{-1}s^{-1}$, laser power 70 mW, grayscale layers 5, minimum power 11.2 mW, power exponent 1.459, mesh z offset 2.1 µm). In **Figures 2**a,b, conventional SEM images detecting secondary electrons are shown. There is no clear difference between the two resists visible and one could not use it to tell which player is in an advantageous position. The absence of visible slicing artifacts, however, indicates that the 2GL printing mode works well and the corresponding parameters are appropriately selected. If we now switch to the VPSE detector to detect emitted photons, we obtain the images shown in Figures 2c,d. Now, the figures and fields printed with the scintillator resist appear white, while the figures consisting of IP-S and the glass substrate around the structure stay dark. This shows, that the scintillator delivers a notably stronger luminescence signal in comparison to glass and IP-S. Now, the black and white figures can be distinguished, but the black figures appear just as silhouettes, and the structural information is lost. Therefore, in Figures 2e,f an overlay of both images above is shown. The luminescence image serves as a mask where the white value of a pixel determines its transparency. Therefore, all the black areas darken the conventional SEM image below. This way, the structural information from the black figures is conserved, but they appear darker and therefore remain distinguishable. Now one can see that the position shows a stalemate if it is white's turn. Additionally, we want to point out that in Figure 2f the knight in the center is printed from the scintillator resin and shows a micrometer resolution on its mane on the back.

3.2. Quantitative Analysis of the Scintillation Efficiency

For a quantitative statement about the scintillation capabilities, the 3D-printed scintillator is compared to a commercial plastic scintillator (Epic-Crystal, EPS100) with a known efficiency of

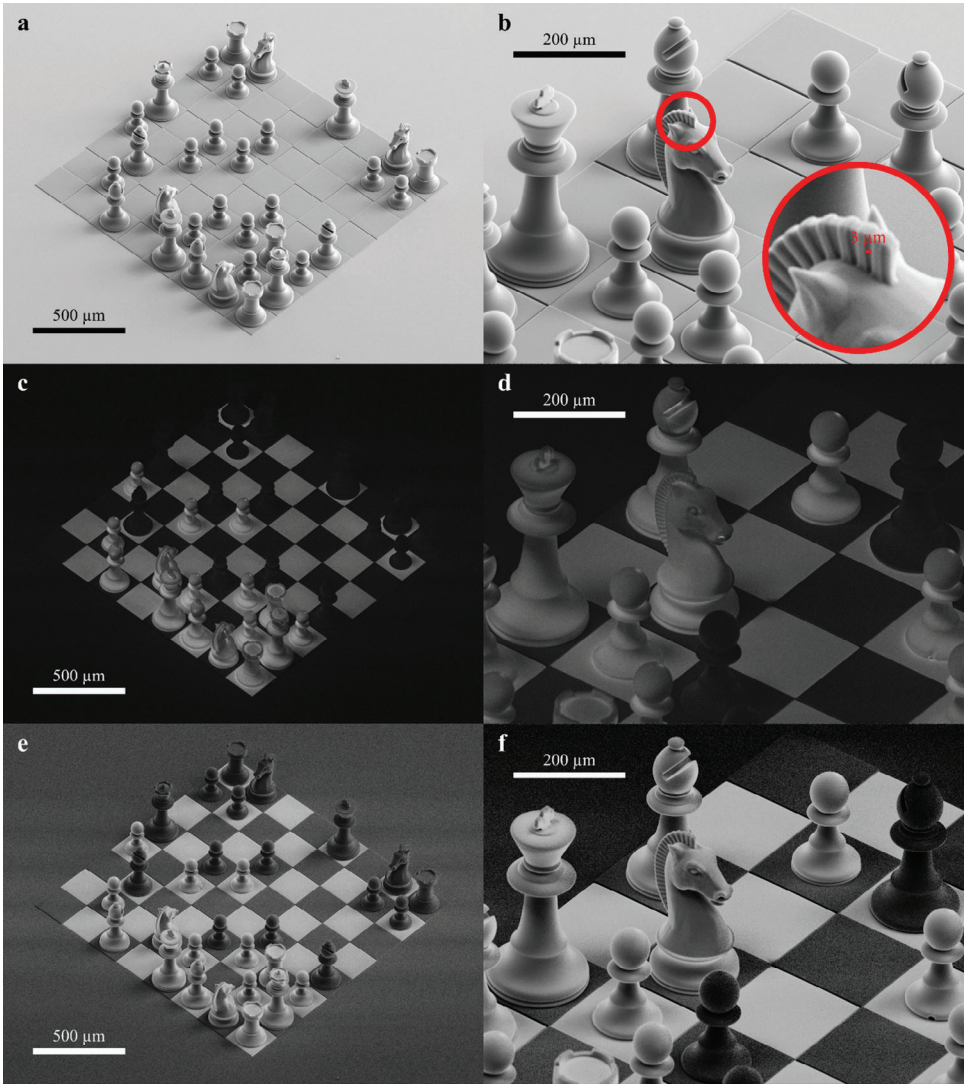

Figure 2. SEM images as a qualitative demonstration of the scintillation capabilities. The chess board at the bottom and the figures are printed from IP-S (black) and the scintillator resin (white), respectively. In the conventional secondary-electron images (a,b), no clear difference between the two types of figures is visible. In panels c and d, the detection method was switched to photons, making the scintillator fields and figures appear bright, while the IP-S structures remain dark. Both channels can be merged in an overlay image e and f, where the luminescence images serve as a mask where transparency scales with the pixel value. Therefore, the scintillator figures and the IP-S figures show all the details from the secondary-electron images, while the brightness of the IP-S figures is still reduced by the overlaying mask. Now all the information is contained in one image and the stalemate position by Sam Loyd (1887) becomes clear.

50–60% anthracene or a light output of 9570 photons MeV^{-1} (using 17400 photons MeV^{-1} for anthracene[37]). For ideal comparison conditions, a 500 µm × 500 µm × 500 µm block of scintillator is printed and the EPS100 is cut to the same size and glued on the same glass substrate. This procedure guarantees equal conditions for both samples. Next, both blocks are investigated under the SEM (detecting photons) using the same settings for contrast and brightness. The primary electron energy was set to 8 keV. The resulting images are shown in **Figure 3a** (EPS100) and Figure 3b (printed scintillator). The average gray values in the regions marked with a red square are 93.1 for the EPS100 and 5.8 for the printed scintillator. A background measurement on a metallic surface was performed and the corresponding gray value of 2.4 has to be subtracted. Next, these gray-value differences are converted into a comparable efficiency by taking the detector's nonlinearity and wavelength dependency (see Section S1, Supporting Information) into account. The emission wavelength of the EPS100 is given in the datasheet as 415 nm, while the emission wavelength of the printed scintillator is estimated from its fluorescence spectrum under excitation with 360 nm as shown in Figure 3c. Here, either the peak wavelength (504.4 nm, red line) or mean wavelength (519.5 nm, black line) can be used for the calculation. The results are a relative efficiency in comparison to the EPS100 of 8.3 or 11.2%, respectively. The difference stems from the spectral-sensitivity dependence of the VPSE photon detector of the SEM. Overall, we estimate that the light output of our printed scintillator material is at ≈930 photons MeV^{-1}.

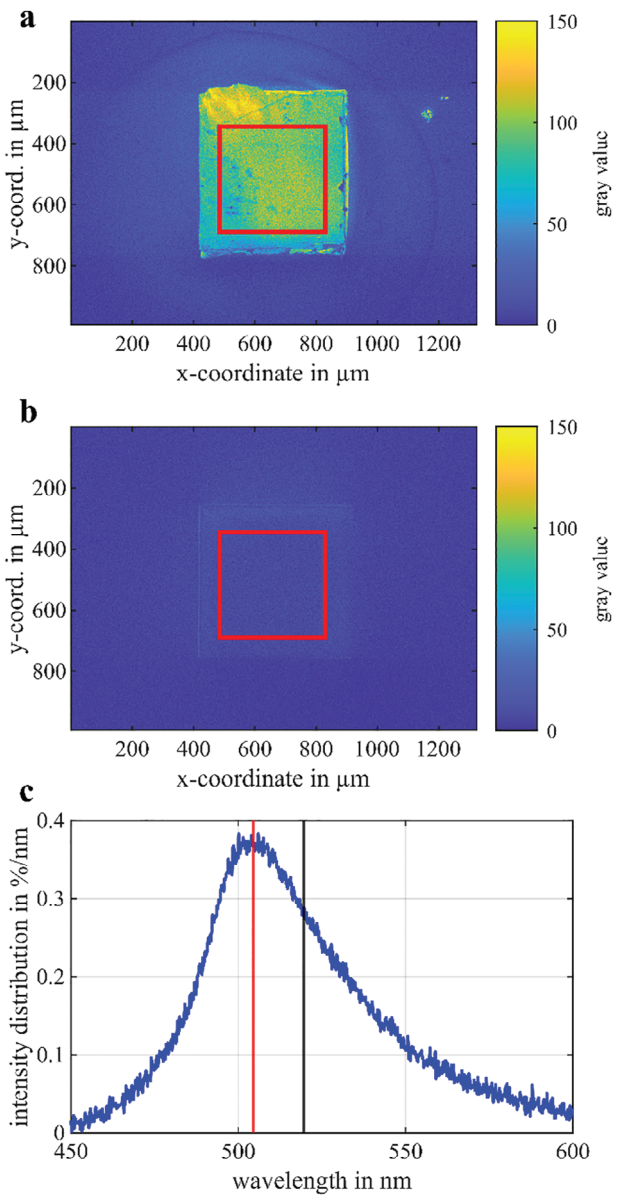

Figure 3. Luminescence images of a 500 µm × 500 µm × 500 µm block of the commercial plastic scintillator EPS100 (a) and our 3D printed scintillator (b). To find the emission wavelength of our printed scintillator the fluorescence spectrum under excitation with 360 nm was measured (c). The peak wavelength is 504.4 nm (red line) and the mean wavelength at 519.5 nm (black line).

4. An Active Transverse Energy Filter as a Possible Application

In this section, we describe an approach to use plastic scintillators as a main component of an angular selective electron detector that is designed to measure electrons with energies of ≈20 keV. Since such a detector system requires complex geometries on the micrometer scale, 3D laser micro-printing is of very high interest.

The Karlsruhe Tritium Neutrino (KATRIN) experiment has the goal of determining the effective electron antineutrino mass with a sensitivity in the vicinity of 0.2 eV @90% C.L.[38] It is based on the ultra-high spectroscopy of electrons from the tritium beta decay at the endpoint of the spectrum with 18.6 keV energy. Recently, KATRIN published its first sub-eV limit on the effective electron anti-neutrino mass of 0.8 eV (90% C.L.), based on the first two high-tritium-activity data-taking campaigns.[39–41]

A limiting factor on KATRIN's final sensitivity stems from a background source originating from its voluminous main spectrometer.[42] It consists of electrons produced not in the tritium decay but which arrive at the detector with indistinguishable energy as the signal electrons but with smaller pitch angles.[20,43] Therefore, designing an angular-selective detector shows great potential for increasing the sensitivity of the KATRIN experiment. The standard approaches for angular measurement of electrons are not applicable in the KATRIN experiment, given the particle's low impact energy of only 18.6 keV and the subsequent short propagation length of a few micrometers within the detector. However, there is an approach to distinguish between the electron angle via the size of their cyclotron radius. This technique is called active transversal energy Filter (aTEF).[20] It proposes a micro-structured detector that acts as a filter for electrons with large cyclotron radii and correspondingly large pitch angles.

Figure 4a shows a schematic view of such a detector and the concept of a transverse energy filter. A possible 3D generalization of such a geometry is shown in a 3D rendering in Figure 4b

Electrons with large cyclotron radii are absorbed by the scintillator and generate a cascade of secondary scintillation photons, which are detected by the photo sensor. Electrons with a small cyclotron radius do not interact with the cell walls and are blocked by a passive layer on top of the scintillator or on the bottom. Thus, they do not give a signal. Given the electro-magnetic environment of the KATRIN detector typical cyclotron radii of signal electrons are ≈150 µm. On the other hand, in building a high-efficiency geometry, the cell wall thickness should be in the range of the electron penetration depth into the material (≈10 µm), ideally with the highest surface quality to fully benefit from the light collection due to total internal reflection. We note that, due to such small dimensions of the scintillator grid, it cannot be produced using conventional manufacturing methods such as e.g., thermal polymerization.

There are at least two approaches to realizing such an angular-sensitive detector, for example by microstructuring Si-PIN diodes via a highly anisotropic cryo-etching procedure.[20] Another approach is an aTEF-detector based on a plastic scintillator that is read out by a CMOS-based single-photon-avalanche-diode (SPAD) array (scint-aTEF) as described in Ref. [42].

To demonstrate the fabrication capabilities of our scintillator system, we printed the aTEF structure on a SPAD array with a cell size of 185 µm × 185 µm × 300 µm and a wall thickness of 30 µm. This resembles the dimensions for an aTEF structure for KATRIN based on a square grid. Figure 4c shows an overlay of such a grid structure with the surface of the SPAD array. After the printing process, two images are taken with an optical microscope. In Figure 4d, one can see that the structure has the desired geometry in comparison to the render, and in Figure 4e also the alignment is visibly correct in comparison to the overlay image. For a more precise view, Figure 4f shows an SEM image that demonstrates the alignment with the SPAD array, indicating sufficient geometrical precision. This example demonstrates the possibility of printing the scintillator directly onto further

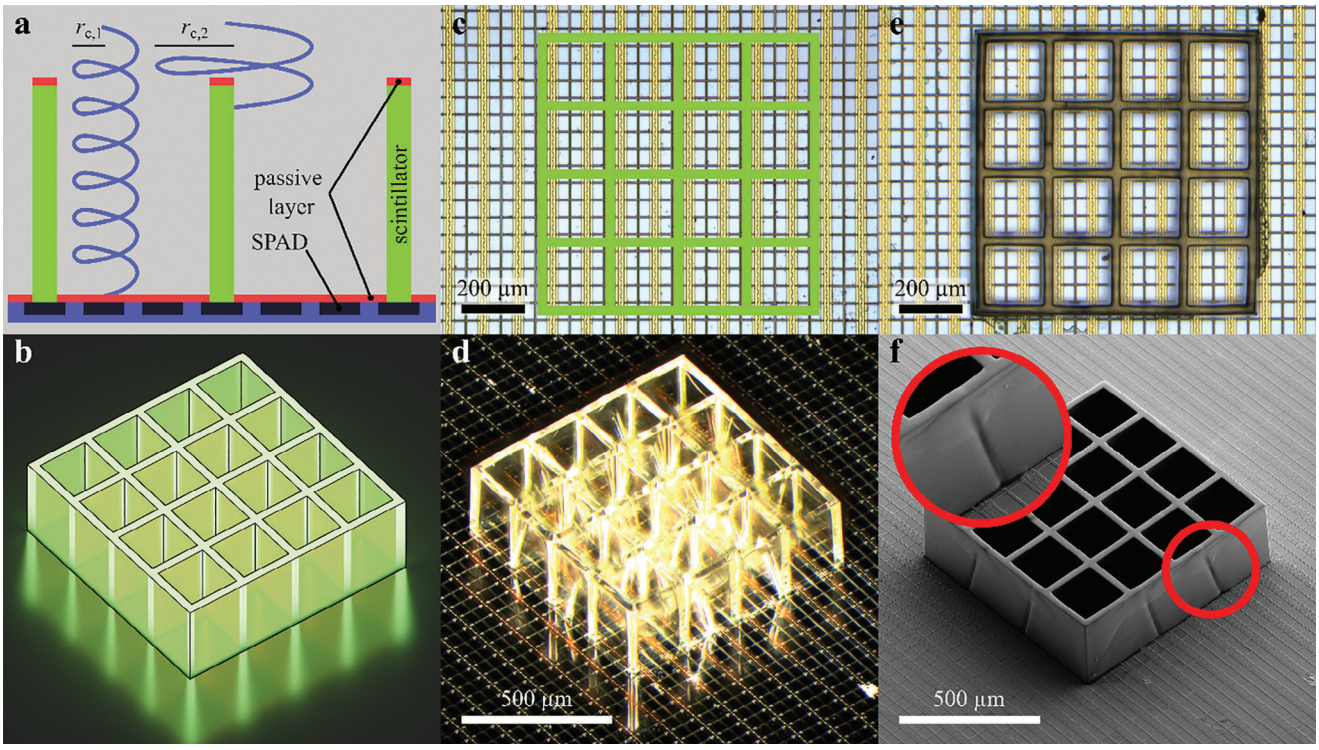

Figure 4. Illustration of the concept of an active Transversal Energy Filter (aTEF) and demonstration of its realizability using a multi-photon printable plastic scintillator. In panel a, the basic concept of filtering is shown. An electron with a low transverse energy, i.e., a small cyclotron radius $r_{c,1}$, does not hit the scintillator material (green) but the passive layer (red) and is therefore not detected. A second electron with a large transverse energy and therefore a large cyclotron radius $r_{c,2} > r_{c,1}$ will hit the walls consisting of scintillator material and therefore generate light. This light is guided to the SPAD array at the bottom by total internal reflection at the optical grade surfaces of the scintillator and can then be detected. A 3D generalization is shown as a render in b. This grid structure can be aligned on a SPAD array as illustrated in c and then directly printed on the SPAD surface using two-photon 3D printing. The results of such a print are shown in panels d and e, under investigation with an optical microscope. The alignment as well as the overall shape match the design requirements. Additionally, an SEM image of the structure has been taken f, also indicating a match with the design. In the SEM image, one can see that the surface is indeed very smooth despite some stitching seams where different writing fields are stitched together. The stitching seams appear under the set shear angle of 15°. If those seams are problematic for a specific application, one has to develop strategies to suppress them as much as possible.

components of the detector system. The requirements of this task, namely a good optical surface quality, a high wall aspect ratio, and a direct and aligned connection to the detector array, are fulfilled simultaneously by 3D laser micro-printing of a scintillating structure. While it might be possible to fabricate similar structures with other fabrication techniques, such as micromolding, the fabrication steps will most likely be way more complicated in order to achieve a result of the same quality.

5. Conclusion

3D printing of plastic scintillators is a field of rapidly growing interest. However, for many applications, for example in the KATRIN experiment, the resolution of the already developed one-photon-based techniques are not sufficient. To close this gap, we developed the first two-photon printable scintillator resin to fabricate 3D high-quality plastic scintillator structures on a micrometer scale. We demonstrated the 3D printing capabilities of this naphthyl- and bisphenol-based resin not only for conventional two-photon polymerization but also with 2GL for fully 3D structures with optical-grade surfaces. For many applications, as the shown aTEF, this is highly advantageous since it enables better control over the generated light, for example, by highly efficient total internal reflection. We also characterized the light output of small scintillator samples using a scanning electron microscope combined with a photodetector. By comparing our scintillator material with a commercially available standard plastic scintillator, we estimate a light output of 930 photons MeV^{-1}, measured at 8 keV incident electron energy. Thus, the light efficiency is significantly lower than the commercial scintillator and also compared to other one-photon-based printed scintillators. We think that the main difference lies in the density of aromatic systems that should be increased with other monomers for better results as suggested by the literature.[19] However, we are optimistic that this number sets a solid foundation for further research in the development of 3D micro-printable plastic scintillators.

To demonstrate the possibility of directly printing our scintillator on a detector, we printed an aTEF structure on a SPAD array. This structure is a real example of a micro-structured scintillator for applications in the KATRIN experiment. For this application, multi-photon laser micro-printing turns out to be a very suitable technology since the scintillator can be printed at very high quality and because the connection to the detectors is very stable and easy to make. With this example, we present one full

detector system out of the many possibilities that become available with micro-structuring plastic scintillators via two-photon 3D laser printing.

All acquired data contributing to this work can be found in our repository under the DOI 10.35097/wtRTyiTkPCSeDheH.

Supporting Information

Supporting Information is available from the Wiley Online Library or from the author.

Acknowledgements

The authors thank Guido Drexlin (Karlsruhe Institute of Technology, Karlsruhe, Germany) for stimulating discussions, Maik Nothdurft (Karlsruhe Institute of Technology, Karlsruhe, Germany) for technical support for cutting small pieces of plastic scintillators, Michael Hippe and Werner Gilde for electronical support in characterizing the VPSE detector in the SEM, and Peter Fischer for the provision of a SPAD (University of Heidelberg, Ziti). The authors acknowledge funding by the Deutsche Forschungsgemeinschaft (DFG, German Research Foundation) under Germany's Excellence Strategy via the Excellence Cluster "3D Matter Made to Order" EXC-2082/1-390761711 (3DMM2O), the Helmholtz Association through the Helmholtz program Materials Systems Engineering (MSE) and by Ministry for Education and Research BMBF (05A23VK2).

Open access funding enabled and organized by Projekt DEAL.

Conflict of Interest

The authors declare no conflict of interest.

Data Availability Statement

The data that support the findings of this study are openly available in Datenpaket: Multi-photon 3D laser micro-printed plastic scintillators for applications in low-energy particle physics at https://doi.org/10.35097/wtRTyiTkPCSeDheH, reference number 35097.

Keywords

2-photon grayscale lithography, 3D laser micro-printing, low energy particle physics, plastic scintillator

Received: July 23, 2024
Revised: September 17, 2024
Published online: October 9, 2024

[1] P. B. Cushman, D. M. Poehlmann, *Plastic Scintillators: Chemistry and Applications* (Ed: M. Hamel), Springer International Publishing, Cham **2021**, p. 541–588.
[2] K. Cankoçak, P. de Barbaro, D. Vishnevskiy, Y. Onel, *J. Phys.: Conf. Ser.* **2009**, *160*, 012055.
[3] F. Cavallari, *J. Phys.: Conf. Ser.* **2011**, *293*, 012001.
[4] P. Cortese, G. Dellacasa, R. Gemme, L. Ramello, M. Sitta, A. Ahmad, N. Ahmad, M. Danish Azmi, M. Irfan, A. Kamal, M. Khan, A. Bilandzic, M. Botje, I. Kraus, M. Krzewicki, P. Kuijer, R. Snellings, N. Van Der Kolk, A. Belogianni, P. Christakoglou, M. Fragkiadakis, P. Ganoti, S. Potirakis, M. Spyropoulou-Stassinaki, C. Tagridis, E. Tsilis, M. Vassiliou, G. E. Bruno, G. D'Erasmo, D. Di Bari, et al., **2008**, https://cds.cern.ch/record/1121574.
[5] T. Lhc. Collaboration, A. A. A. Jr, L. M. A. Filho, A. F. Barbosa, I. Bediaga, G. Cernicchiaro, G. Guerrer, H. P. L. Jr, A. A. Machado, J. Magnin, F. Marujo, J. M. de Miranda, A. Reis, A. Santos, A. Toledo, K. Akiba, S. Amato, B. de Paula, L. de Paula, T. da Silva, M. Gandelman, J. H. Lopes, B. Maréchal, D. Moraes, E. Polycarpo, F. Rodrigues, J. Ballansat, Y. Bastian, D. Boget, I. D. Bonis, V. Coco, et al., *J. Inst.* **2008**, *3*, S08005.
[6] D. G. Michael, P. Adamson, T. Alexopoulos, W. W. M. Allison, G. J. Alner, K. Anderson, C. Andreopoulos, M. Andrews, R. Andrews, C. Arroyo, S. Avvakumov, D. S. Ayres, B. Baller, B. Barish, M. A. Barker, P. D. Barnes, G. Barr, W. L. Barrett, E. Beall, K. Bechtol, B. R. Becker, A. Belias, T. Bergfeld, R. H. Bernstein, D. Bhattacharya, M. Bishai, A. Blake, V. Bocean, B. Bock, G. J. Bock, et al., *Nucl. Instrum. Methods Phys. Res., Sect. A* **2008**, *596*, 190.
[7] D. S. Ayres, G. R. Drake, M. C. Goodman, J. J. Grudzinski, V. J. Guarino, R. L. Talaga, A. Zhao, P. Stamoulis, E. Stiliaris, G. Tzanakos, M. Zois, *The NOνA Technical Design Report*, Fermi National Accelerator Lab. (FNAL), Batavia, IL, USA **2007**.
[8] L. Aliaga, O. Altinok, C. Araujo Del Castillo, L. Bagby, L. Bellantoni, W. F. Bergan, A. Bodek, R. Bradford, A. Bravar, H. Budd, A. Butkevich, D. A. Martinez Caicedo, M. F. Carneiro, M. E. Christy, J. Chvojka, H. da Motta, J. Devan, G. A. Díaz, S. A. Dytman, B. Eberly, J. Felix, L. Fields, R. Fine, R. Flight, A. M. Gago, C. Gingu, T. Golan, A. Gomez, R. Gran, D. A. Harris, et al., *Nucl. Instrum. Methods Phys. Res., Sect. A* **2015**, *789*, 28.
[9] Y. Poirier, J. Xu, S. Mossahebi, F. Therriault-Proulx, A. Sawant, *Med Phys* **2022**, *49*, 4682.
[10] P. Moskal, E. Ł. Stępień, *PET Clin* **2020**, *15*, 439.
[11] E. Timakova, M. Bazalova-Carter, S. Zavgorodni, *Phys Med Biol* **2023**, *68*, 175040.
[12] E. Ciarrocchi, E. Ravera, A. Cavalieri, M. Celentano, D. Del Sarto, F. Di Martino, S. Linsalata, M. Massa, L. Masturzo, A. Moggi, M. Morrocchi, J. H. Pensavalle, M. G. Bisogni, *Phys Med* **2024**, *121*, 103360.
[13] H. Yang, G. Luo, T. Yu, S. Zhao, B. Hu, Z. Huang, H. Shen, L. Yang, Y. Chen, J. Tang, *Nucl. Instrum. Methods Phys. Res., Sect. A* **2022**, *1042*, 167402.
[14] G. Konstantinou, P. Lecoq, J. M. Benlloch, A. J. Gonzalez, *IEEE Trans Radiat Plasma Med Sci* **2022**, *6*, 5.
[15] Z. Lin, S. Lv, Z. Yang, J. Qiu, S. Zhou, *Adv. Sci.* **2022**, *9*, 2102439.
[16] G. Konstantinou, L. Zhang, D. Bonifacio, R. Latella, J. M. Benlloch, A. J. Gonzalez, P. Lecoq, *IEEE Trans Radiat Plasma Med Sci* **2024**, *8*, 482.
[17] S. Kim, Y. H. Seoung, *J Korean Phys Soc* **2019**, *75*, 953.
[18] J. Son, D. G. Kim, S. Lee, J. Park, Y. Kim, T. Schaarschmidt, Y. K. Kim, *J Korean Phys Soc* **2018**, *73*, 887.
[19] D. G. Kim, K. Kim, S. Lee, Y. K. Kim, *Radiat. Phys. Chem.* **2022**, *198*, 110255.
[20] K. Gauda, S. Schneidewind, G. Drexlin, A. Fulst, V. Hannen, T. König, A. Lokhov, P. Oelpmann, H. W. Ortjohann, W. Pernice, R. G. H. Robertson, R. W. J. Salomon, M. Stappers, C. Weinheimer, *Eur. Phys. J. C* **2022**, *82*, 922.
[21] V. Hahn, P. Kiefer, T. Frenzel, J. Qu, E. Blasco, C. Barner-Kowollik, M. Wegener, *Adv. Funct. Mater.* **2020**, *30*, 1907795.
[22] S. Rodríguez, *PhotonicsViews* **2020**, *17*, 36.
[23] T. Aderneuer, O. Fernández, R. Ferrini, *Opt. Express* **2021**, *29*, 39511.
[24] L. Siegle, S. Ristok, H. Giessen, *Opt. Express* **2023**, *31*, 4179.
[25] Q. Li, V. Raimbault, P. F. Calmon, B. Reig, P. Debernardi, H. Ottevaere, J. B. Doucet, J. Roul, V. Bardinal, *J. Opt. Microsyst.* **2023**, *3*, 033501.
[26] M. He, X. Shen, X. Liu, C. Kuang, X. Liu, *Opt. Lett.* **2023**, *48*, 5221.
[27] F. Xie, L. Liang, Q. Zhou, M. Jiang, L. P. Sun, L. Jin, X. Li, Y. Cao, *Opt. Laser Technol.* **2024**, *175*, 110762.
[28] W. Hadibrata, H. Wei, S. Krishnaswamy, K. Aydin, *Nano Lett.* **2021**, *21*, 2422.

[29] P. I. Dietrich, M. Blaicher, I. Reuter, M. Billah, T. Hoose, A. Hofmann, C. Caer, R. Dangel, B. Offrein, U. Troppenz, M. Moehrle, W. Freude, C. Koos, *Nat. Photonics* **2018**, *12*, 241.
[30] P. Fischer, R. K. Zimmermann, B. Maisano, *Nucl. Instrum. Methods Phys. Res., Sect. A* **2022**, *1040*, 167033.
[31] T. Baldacchini, C. N. LaFratta, R. A. Farrer, M. C. Teich, B. E. A. Saleh, M. J. Naughton, J. T. Fourkas, *J. Appl. Phys.* **2004**, *95*, 6072.
[32] L. Jiang, W. Xiong, Y. Zhou, Y. Liu, X. Huang, D. Li, T. Baldacchini, L. Jiang, Y. Lu, *Opt. Express* **2016**, *24*, 13687.
[33] J. Tang, X. Xu, X. Shen, C. Kuang, H. Chen, M. Shi, N. Huang, *ACS Appl Polym Mater* **2023**, *5*, 2956.
[34] Y. Zhang, Y. Su, Y. Zhao, Z. Wang, C. Wang, *Small* **2022**, *18*, 2200514.
[35] A. Mauri, P. Kiefer, P. Neidinger, T. Messer, N. M. Bojanowski, L. Yang, S. Walden, A. N. Unterreiner, C. Barner-Kowollik, M. Wegener, W. Wenzel, M. Kozlowska, *Chem. Sci.* **2024**, *15*, 12695.
[36] NanoGuide, https://support.nanoscribe.com/hc/en-gb (accessed: May 2024).
[37] C. Buck, B. Gramlich, M. Lindner, C. Roca, S. Schoppmann, *J. Inst.* **2019**, *14*, P01027.
[38] T. K. collaboration, M. Aker, K. Altenmüller, J. F. Amsbaugh, M. Arenz, M. Babutzka, J. Bast, S. Bauer, H. Bechtler, M. Beck, A. Beglarian, J. Behrens, B. Bender, R. Berendes, A. Berlev, U. Besserer, C. Bettin, B. Bieringer, K. Blaum, F. Block, S. Bobien, M. Böttcher, J. Bohn, K. Bokeloh, H. Bolz, B. Bornschein, L. Bornschein, H. Bouquet, N. M. Boyd, T. Brunst, et al., *J. Inst.* **2021**, *16*, T08015.
[39] KATRIN Collaboration, M. Aker, K. Altenmüller, M. Arenz, M. Babutzka, J. Barrett, S. Bauer, M. Beck, A. Beglarian, J. Behrens, T. Bergmann, U. Besserer, K. Blaum, F. Block, S. Bobien, K. Bokeloh, J. Bonn, B. Bornschein, L. Bornschein, H. Bouquet, T. Brunst, T. S. Caldwell, L. La Cascio, S. Chilingaryan, W. Choi, T. J. Corona, K. Debowski, M. Deffert, M. Descher, P. J. Doe, et al., *Phys. Rev. Lett.* **2019**, *123*, 221802.
[40] KATRIN Collaboration, M. Aker, K. Altenmüller, A. Beglarian, J. Behrens, A. Berlev, U. Besserer, B. Bieringer, K. Blaum, F. Block, B. Bornschein, L. Bornschein, M. Böttcher, T. Brunst, T. S. Caldwell, L. La Cascio, S. Chilingaryan, W. Choi, D. Díaz Barrero, K. Debowski, M. Deffert, M. Descher, P. J. Doe, O. Dragoun, G. Drexlin, S. Dyba, F. Edzards, K. Eitel, E. Ellinger, R. Engel, et al., *Phys Rev D* **2021**, *104*, 012005.
[41] M. Aker, A. Beglarian, J. Behrens, A. Berlev, U. Besserer, B. Bieringer, F. Block, S. Bobien, M. Böttcher, B. Bornschein, L. Bornschein, T. Brunst, T. S. Caldwell, R. M. D. Carney, L. La Cascio, S. Chilingaryan, W. Choi, K. Debowski, M. Deffert, M. Descher, D. Díaz Barrero, P. J. Doe, O. Dragoun, G. Drexlin, K. Eitel, E. Ellinger, R. Engel, S. Enomoto, et al., *Nat. Phys.* **2022**, *18*, 160.
[42] M. Aker, M. Balzer, D. Batzler, A. Beglarian, J. Behrens, A. Berlev, U. Besserer, M. Biassoni, B. Bieringer, F. Block, S. Bobien, L. Bombelli, D. Bormann, B. Bornschein, L. Bornschein, M. Böttcher, C. Brofferio, C. Bruch, T. Brunst, T. S. Caldwell, M. Carminati, R. M. D. Carney, S. Chilingaryan, W. Choi, O. Cremonesi, K. Debowski, M. Descher, D. D. Barrero, P. J. Doe, O. Dragoun, et al., *J. Phys. G: Nucl. Part. Phys.* **2022**, *49*, 100501.
[43] A. Lokhov, B. Bieringer, G. Drexlin, S. Dyba, K. Gauda, F. Fränkle, F. Glück, V. Hannen, D. Hinz, S. Mertens, C. Rodenbeck, A. Schaller, C. Weinheimer, *Eur. Phys. J. C* **2022**, *82*, 258.